

Inference of the neutron star equation of state from cosmological distances

Carl-Johan Haster,^{1,2} Katerina Chatziioannou,³ Andreas Bauswein,⁴ and James Alexander Clark⁵

¹*LIGO Laboratory, Massachusetts Institute of Technology, 185 Albany St, Cambridge, MA 02139, USA*

²*Department of Physics and Kavli Institute for Astrophysics and Space Research, Massachusetts Institute of Technology, 77 Massachusetts Ave, Cambridge, MA 02139, USA*

³*Center for Computational Astrophysics, Flatiron Institute, 162 5th Ave, New York, NY 10010, USA*

⁴*GSI Helmholtzzentrum für Schwerionenforschung, Planckstraße 1, 64291 Darmstadt, Germany*

⁵*Center for Relativistic Astrophysics and School of Physics, Georgia Institute of Technology, Atlanta, GA 30332*

Finite-size effects on the gravitational wave signal from a neutron star merger typically manifest at high frequencies where detector sensitivity decreases. Proposed sensitivity improvements can give us access both to stronger signals and to a myriad of weak signals from cosmological distances. The latter will outnumber the former and the relevant part of signal will be redshifted towards the detector most sensitive band. We study the redshift dependence of information about neutron star matter and find that single-scale properties, such as the star radius or the post-merger frequency, are better measured from the distant weak sources from $z \sim 1$.

INTRODUCTION

The gravitational wave (GW) signal emitted during the coalescence of two neutron stars (NSs) carries the imprint of the equation of state (EoS) of cold, supranuclear matter [1, 2]. Extracting EoS attributes is a key science goal not only of GW astronomy, but also of diverse probes such as nuclear experiment and theory, and radio and X-ray observations of pulsars [3–7]. To date, GWs from two binary neutron star (BNS) coalescences have been detected [8–11] and combined with other constraints to study the EoS, e.g. [10, 12–16]. Projections from simulated observations suggest GWs will dominate the astrophysical EoS constraints in the next ~ 5 years [16].

Ground-based GW detectors observe a BNS coalescence signal for multiple minutes, starting at ~ 10 – 20 Hz and sweeping up in frequency towards merger. The lower frequency cutoff is predominantly determined by the detector sensitivity. The final, high frequency part of the signal nominally falls within the detector bandwidth, but depending on the system mass and EoS the decreased detector sensitivity might make its accurate extraction challenging in the near future. The signal up to a few hundred Hz is not expected to inform NS EoS constraints as the inspiraling bodies are sufficiently separated such that matter effects are subdominant (excluding potential resonant effects [17, 18], instabilities [19, 20], etc.); they scale as $(R/r)^5$, where R is the NS radius and r the binary separation [21].

Once the NSs are sufficiently close and the signal reaches a few hundred Hz, mutual tidal interactions induce quadrupole moments on each star. The additional quadrupole moment (besides the orbital one) affects both the binding energy and the rate of energy extraction, effectively speeding up the system evolution towards merger. This speed-up depends on the NSs size (less compact NSs are generally more deformable) and can be measured from the phase evolution of the signal, constraining the NSs deformability. Depending on the NS mass and

radius, the part of the signal influenced by tidal interactions corresponds to frequencies $\gtrsim 400$ Hz in the source frame of the BNS. After the inevitable collision, and unless it promptly forms a BH, the merger remnant emits a signal dominated by a single frequency component, usually at 1500 – 4000 Hz [22–36]. This mode has been linked to f-modes of the remnant star [37, 38]; it depends on the remnant’s density, so it can offer complementary information about the EoS stiffness. For more massive NSs or for stiffer EoSs the dominant frequency is lower and the signal is easier to extract from the noise [28].

The two observed BNS signals already constrain tidal interactions between the coalescing NSs [9, 10, 39, 40], but the post-merger signal was lost in the detector noise [9, 41]. Planned improvements of GW detectors [42–45] will not only allow for better tidal measurements, but might also reveal the elusive post-merger signal [46–50]. Further ahead, next generation detectors [51–55] predict a $\mathcal{O}(10)$ sensitivity increase, potentially detecting and individually resolving a significant fraction of all BNS coalescences even at cosmological distances [56], occurring every $\mathcal{O}(10s)$ [57].

The cosmological reach of next generation detectors results in observations with non-negligible redshifting compared to the emitted signal. Cosmological redshifting is familiar in GW astronomy as even current-sensitivity binary black hole (BBH) signals are appreciably redshifted [58]. This can be a blessing and a curse for BBHs as redshifting simultaneously amplifies the signal (since masses appear larger) and shifts it to lower frequencies, potentially outside the detectors’ sensitive band. Observed BNS signals will also appear more massive and lower in frequency, resulting in some early inspiral signal being lost to low-frequency noise. However, for the typical BNS reach of next generation detectors, $z \sim 2$ – 3 , this early signal is generally not informative about finite-size effects. The late inspiral and post-merger signals are typically emitted above 400 Hz, so even a serendipitous detection at $z = 10$ would redshift the signal to $\gtrsim 35$ Hz, safely

above the noise dominated frequencies. Figure 1 shows the observed pre-merger (top) and post-merger (bottom) BNS signal at different redshifts compared to various detector noise spectra. Both signals move to lower frequencies with increasing redshift, but always above 10Hz.

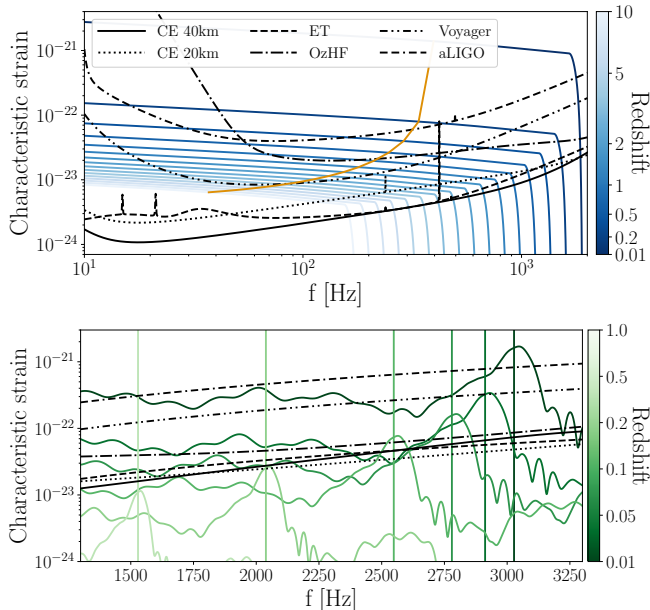


FIG. 1. Characteristic strain [59] of a source-frame $1.362 + 1.362M_{\odot}$ BNS signal at different redshifts (shaded blue or green) and planned or proposed detectors (black lines). *Top panel*: Late-inspiral signal assuming the H4 EoS [60]. The orange line represents 400Hz in the source frame; the tidally-corrected signal is always observed with $f > 10\text{Hz}$. *Bottom panel*: Post-merger signal assuming EoS7 from [49]. Vertical lines mark the dominant post-merger frequency.

Besides redshifting, distant sources are also more numerous due to volume effects. The number of binaries per time, per redshift slice in the observer frame is

$$R(z) = \frac{dN}{dTdz} = \frac{R_s(z) dV_c}{1+z dz}, \quad (1)$$

where dV_c/dz is the differential comoving volume, $R_s(z)$ is the rate per comoving volume in the source frame, and the $1+z$ term converts from the source frame to the observer frame. We assume $R_s(z)$ has the same shape as the star formation rate [61], which peaks at $z \sim 2$ and corresponds to an effective zero delay time between binary formation and merger. A nonzero delay time would smoothen the redshift-dependent rate, making it less peaked than the star formation rate. We assume a local BNS merger rate as $R_s(z=0) = 500\text{Gpc}^{-3}\text{yr}^{-1}$, consistent with current BNS observations [11].

We study whether the fewer, loud, close-by signals or the numerous, weak, distant, redshifted signals offer the most information about the NS EoS. Expectedly, the answer depends on the detector cosmological reach. Next-generation detectors can extract a single EoS scale, such

as the NS radius at a fiducial mass or the frequency of the post-merger oscillations, better with the multitude of far-away sources, thanks to appreciable nonlocal information. Conversely, detailed features of the EoS such as the functional dependence of tidal properties and radius on the mass require the simultaneous extraction of multiple parameters and constraints are dominated by the few loud sources from the local Universe.

PRE-MERGER SIGNAL

During the late inspiral phase of a BNS coalescence, matter effects are encoded in the parameter Λ quantifying the tidal deformation of a NS under an external field [21, 62, 63]. We estimate the expected information gained from measuring the tidally-corrected signal and Λ through the Fisher information matrix F [64]. The accumulated information can be approximated by $\det F$, the determinant of F which scales with the observed signal-to-noise ratio (SNR) as $\det F \sim \text{SNR}^{2D}$, where D is the number of relevant parameters [65]. For $D = 1$ this reduces to the well known SNR^2 dependence on the measurement covariance and the expectation that SNR adds in quadrature rather than linearly.

Λ depends on the NS mass m , so to accurately characterize a generic $\Lambda(m)$ curve, D is in principle large. In practice, generic EoSs can be approximated with a few parameters only. For hadronic EoSs, only a single parameter is expected to be measurable with second generation detectors, for example $\Lambda(m = 1.4M_{\odot})$ [66]. Such a measurement would only provide a single scale of the EoS, such as the radius at a specific NS mass. EoS-insensitive relations also suggest that hadronic EoSs can be suitably described by a single parameter [39, 67–70]. Instead, exploring features of the EoS, such as the mass dependence of the tidal parameter or the presence of a phase transition [71–75], relies on EoS parametrizations. Common models employ ~ 4 or more parameters [76–82] with additional parameters for eventual phase transitions [82–84]. With this in mind we present results for $D = \{1, 2\}$.

We simulate signals from one year’s worth of nonspinning BNS coalescences with the redshift distribution of Eq. 1. We use WFF1 [85], SLY2 [86, 87], and H4 [60] as fiducial EoSs with varying stiffness, but consistent with GW170817 [10, 88]. We assume two source frame mass distributions: (i) masses are drawn uniformly in $[1, M_{\text{max}}]M_{\odot}$, where M_{max} is the assumed EoS maximum mass, and (ii) the primary mass is drawn from a bimodal distribution [89] with a mass ratio q distribution $\sim q^3$ [90]. We distribute systems uniformly across the sky and binary orientations and retain systems with single-detector SNR above 8, evaluated from 10Hz with the waveform model IMRPHENOMPv2_NRTIDAL [91] and the proposed 40km Cosmic Explorer (CE) instrument [51–53](CE2 from [92]). For EoS inference we only

consider the SNR above 400Hz in the source frame (orange line in Fig. 1) restricting to the tidally-corrected signal. Figure 2 shows the total information per redshift slice per year for $D = \{1, 2\}$; at each redshift bin we add SNR^{2D} from detectable binaries, collecting the total information by systems at that distance.

For the inspiral signal in the stationary phase approximation [93], the SNR is proportional to $\mathcal{M}^{5/6}/D_L \sim (1+z)^{5/6}/D_L$, where D_L is the luminosity distance and $\mathcal{M} \equiv (m_1 m_2)^{3/5} (m_1 + m_2)^{-1/5}$ is the source-frame chirp mass. As D_L increases, the denominator increases linearly; distant signals are weaker. Simultaneously, the redshifted mass is higher than the source-frame mass resulting in a higher signal amplitude and there are more sources at large distances; the SNR^2 distribution peaks at $z \sim 1$. The SNR^4 distribution, on the other hand, is a monotonically decreasing function, as the $\sim 1/D_L^4$ decline cannot be compensated by either redshifting or volume effects. For $D = 1$, corresponding to measuring a single EoS scale, information is dominated by events at $z \sim 1$. For $D > 1$ the distribution peaks at $z = 0$ and rare loud events dominate, consistent with [77].

Besides the differing shapes of the distributions, the total accumulated SNR is also higher for $D = 1$ for all EoSs and mass distributions. For a set of N observations, the total SNR grows as $N^{1/(2D)}$, suggesting a more efficient collection of information for lower-dimensional analyses. The effect of the assumed mass distribution and EoS is smaller, though as expected we find that the uniform mass distribution leads to larger SNRs as it contains a larger fraction of massive NSs. Stiff EoSs – such as H4 – predict large NS radii for a given mass and hence an earlier tidal disruption relative to a softer EoS, corresponding to a small reduction in SNR.

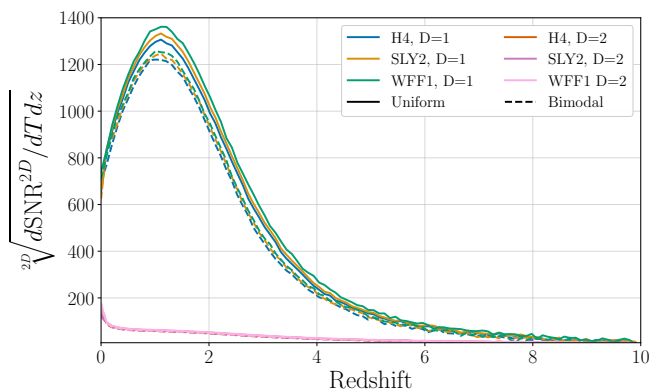


FIG. 2. Total pre-merger SNR distribution per year per redshift slice, as a function of redshift for two mass distributions, three EoSs, $D = \{1, 2\}$, and the 40km CE detector. For $D = 1$, the available SNR is dominated by BNSs at cosmological distances. For $D = 2$, the accumulated information peaks at $z \sim 0$, suggesting a main contribution from local sources.

POST-MERGER SIGNAL

The post-merger signal is dominated by a single frequency component, see Fig. 1, that depends on the EoS stiffness. Subdominant structure also exists [37, 94], but the main subdominant modes are related to the dominant one [32, 95]. We therefore use $D = 1$ and follow a similar procedure as above, using only systems detectable by their pre-merger signal. For the detected post-merger signal we employ equal-mass simulations with EoS6, EoS7, and EoS4 from [49], constructed to be consistent with GW170817 [10]. Simulations were performed with a relativistic smooth particle hydrodynamics code, with conformal flatness to solve the Einstein equations [96–99].

We assume the same mass and orientation distribution as above. The amplitude of the post-merger signal is generally expected to increase with mass and drop steeply when the total mass M approaches the threshold for prompt BH formation. Reference [100] presents a phenomenological model for the post-merger signal with the amplitude proportional to M though with some residual dependence on q [100–102]. Our signals are based on numerical simulations with a certain M [49]; to estimate the observed signal from a binary with a different M and z , we scale the amplitude proportionally to the redshifted M [100]. We also adjust the dominant frequency inversely proportionally to the system’s redshifted M . Finally, systems whose mass exceeds an EoS-dependent threshold result in prompt collapse to a BH, emitting negligible signal. We use the relations in [103, 104] to quantify this threshold for each EoS and discard systems exceeding it by setting their post-merger SNR to zero.

Figure 3 shows the total information as a function of the redshift for all EoSs and mass distributions. We find that the available post-merger SNR is dominated by nonlocal sources with a distribution peaking at $z \sim 1$. The uniform mass distribution results in overall larger detected SNR, as it results in heavier systems and louder signals. Additionally, stiffer EoSs generally result in a higher total SNR as their post-merger frequency is lower. However, the threshold mass is also important, as a low threshold to prompt collapse means that the heavier (and hence potentially louder) systems emit no relevant signal. As a result of this tradeoff, the stiffest EoS in our set, EoS4, indeed results in the highest SNR, but there is no clear distinction between EoS6 and EoS7.

Finally, we comment on a phenomenon observed in [49]. Depending on the shape of the post-merger spectrum and the steepness of the detector noise, the lower-frequency subdominant modes might result in higher SNR than the dominant one, leading to a “reversal” in which is observed first. Combining multiple sources at different masses and redshifts could help mitigate any potential confusion arising from a misidentification of the dominant mode from a loud source.

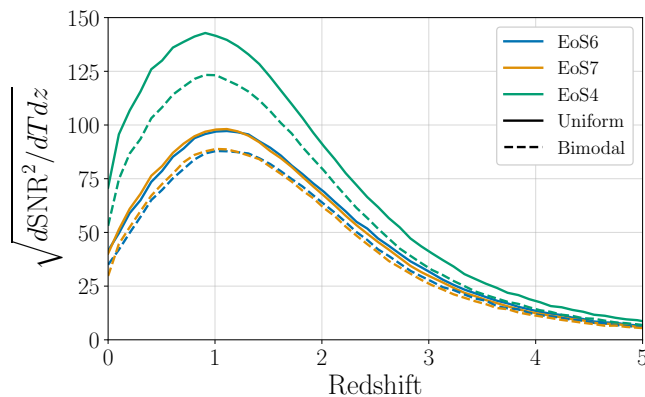


FIG. 3. Total post-merger SNR distribution per year per redshift slice as a function of redshift for two mass distributions, three EoSs and the 40km CE detector ($D = 1$). The distribution peaks at $z \sim 1$, suggesting a significant contribution from nonlocal sources on the total post-merger information.

EFFECT OF DETECTOR CONFIGURATION

The conclusion that nonlocal binaries contribute significant information about finite-size effects hinges on detectors with cosmological reach for BNSs that can detect signals out to redshift $z \gtrsim 1$. To explore this effect, we repeat the above analyses with five additional detector configurations, see Fig. 1. Besides the 40km CE detector, we also study its 20km version [51, 105] with nominally greater sensitivity at frequencies above 2kHz [106] compared to the 40km version. We also include the Einstein Telescope (ET) [54, 55, 107] (in its ET-D configuration), a LIGO Voyager detector [107, 108] and Advanced LIGO (aLIGO) at its final design sensitivity [109, 110]. Finally, we include OzHF [111, 112], a proposed detector designed for dedicated high-frequency GW observations.

The total pre-merger information with each detector configuration is shown in Fig. 4, for a single-parameter analysis assuming the bimodal mass distribution and the H4 EoS. The next generation instruments CE and ET detect BNS signals at cosmological distances, and nonlocal sources from $z \sim 1$ dominate the accumulated information due to volume and redshifting effects. For detectors that cannot detect the myriad of distant binaries, though, the available SNR is dominated by rare loud signals.

The area under the square of each curve in Fig. 4 corresponds to the total information, or total SNR^2 , collected during one year of observation. By comparing the relative information gained between different detectors we can gauge their respective contributions towards a characterization of the NS EoS. Table I presents the relative information gained from each detector compared to CE 40km for pre-merger ($D = \{1, 2\}$) and post-merger signals. The ratios amount to years of observation with each detector to match one year of CE 40km observation, or

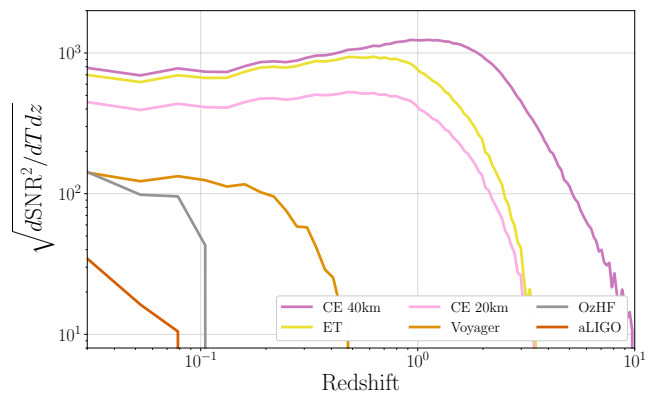


FIG. 4. Total pre-merger SNR distribution per year per redshift slice, as a function of redshift for the bimodal mass distribution, the H4 EoS and for different planned or proposed detectors. We show results for $D = 1$.

Detector	Pre-merger, D=1	Pre-merger, D=2	Post-merger, D=1
CE 40km	1	1	1
ET	3	2	9
CE 20km	10	12	3
Voyager	830	1400	1200
OzHF	2700	1100	450
aLIGO	64000	170000	42000

TABLE I. Relative information $\sim \text{SNR}^{2D}$ gained from each detector compared to CE 40km. We use results with the bimodal mass distribution and EoSs H4 and EoS7 for the pre-merger and post-merger signals respectively.

equivalently how many detectors of a certain class would be required to match a single CE 40km instrument.

Third generation detectors offer at least an order of magnitude more information about both pre-merger and post-merger signals compared to non-cosmological BNS detectors. The increased high-frequency sensitivity for the 20km CE configuration results in approximately similar performance compared to its 40km counterpart for post-merger signals, though not for pre-merger ones. “2.5”G detectors such as OzHF and Voyager offer a clear improvement over aLIGO, and could potentially lead to a post-merger detection (total $\text{SNR} \gtrsim 5$) and stringent pre-merger EoS constraints (total $\text{SNR} \gtrsim 33$ (60) with $D = 1$ and $\gtrsim 16$ (15) with $D = 2$ for OzHF (Voyager)).

DISCUSSION

Over the next decade the sensitivity of GW detectors will increase, allowing for detection of a large population of BNSs at cosmological distances. These observations are aided by the redshift dependent merger rate as well as cosmological redshifting of the observed signals. With a conservative detection threshold of $\text{SNR} > 8$ in one 40km

CE detector, we find $\sim 1/3$ of all BNSs in the Universe are individually detectable. In terms of SNR, they correspond to about 60% of the total available SNR from all mergers, as the undetected signals are intrinsically weak and subdominant thanks to the $N^{1/2}$ SNR scaling. The detection procedure deployed for real GW observations is more sophisticated [113, 114], including a global network of GW detectors and potentially being able to characterize not only the individually resolvable signals but also a stochastic background [56, 57, 115]. These effects could increase the available information.

Measurement of a single scale of the NS EoS (such as the neutron star radius or the frequency of post-merger oscillations) is dominated by information from the population of BNSs at $z \sim 1$ for third-generation GW detectors. Current facilities, on the other hand, are inherently insensitive to such a distant source population and constraints are dominated by nearby sources. This suggests that EoS constraints benefit from both high and low frequency sensitivity: the high part offers direct information about finite-size effects, and the low part contributes towards the detection of the distant BNS population in the first place. Extraction of more than one EoS parameter, for example to detect the presence of a phase transition [84, 116], is also primarily achieved by the few BNS sources at high individual SNR in the local Universe. The cosmological reach of third-generation detectors and the large recovered SNR for the tidally-corrected signal are essential for simultaneous EoS and cosmological inference even beyond the Hubble parameter [117–119].

The large total SNR available to next generation detectors raises the bar for mitigating systematic biases. Whether the SNR comes from a single loud source [120–122] or is the cumulative result of many weak sources [122], accurate waveform models describing any individual BNS signal are essential for unbiased estimates of the system parameters. The post-merger signal is amenable to morphology independent studies with less stringent accuracy requirements [48]. In parallel, interpreting tidal and post-merger measurements hinges on EoS representations or universal relations. Ongoing work on improved waveform models, numerical simulations, and understanding of the EoS is essential for achieving the full potential of next-generation GW detectors.

The authors would like to thank Tom Callister for useful discussions. We also thank Daniel Brown for providing the OzHF sensitivity curve, and Evan Hall for providing the CE 20km sensitivity curve. C.-J.H. acknowledge support of the National Science Foundation, and the LIGO Laboratory. A.B. acknowledges support by the European Research Council (ERC) under the European Union’s Horizon 2020 research and innovation programme under grant agreement No. 759253. A.B. and by Deutsche Forschungsgemeinschaft (DFG, German Research Foundation) – Project-ID 279384907 – SFB 1245 and Project-ID 138713538 – SFB 881 (“The

Milky Way System”, subproject A10). J.A.C. acknowledge support of the National Science Foundation Grants PHY-1700765, OAC-1841530 and PHY-1809572. LIGO was constructed by the California Institute of Technology and Massachusetts Institute of Technology with funding from the National Science Foundation and operates under cooperative agreement PHY-1764464. The Flatiron Institute is supported by the Simons Foundation. The authors are grateful for computational resources provided by the LIGO Laboratory and supported by National Science Foundation Grants PHY-0757058 and PHY-0823459. This analysis was made possible by the LALSuite [123], astropy [124, 125], numpy [126], SciPy [127] and matplotlib [128] software packages. This article carries LIGO Document Number LIGO-P2000143.

-
- [1] J. A. Faber and F. A. Rasio, *Living Reviews in Relativity* **15**, 8 (2012).
 - [2] L. Baiotti and L. Rezzolla, *Rept. Prog. Phys.* **80**, 096901 (2017), [arXiv:1607.03540 \[gr-qc\]](#).
 - [3] J. M. Lattimer and B. F. Schutz, *The Astrophysical Journal* **629**, 979 (2005).
 - [4] J. Antoniadis, P. C. Freire, N. Wex, T. M. Tauris, R. S. Lynch, *et al.*, *Science* **340**, 1233232 (2013), [arXiv:1304.6875 \[astro-ph.HE\]](#).
 - [5] M. C. Miller and F. K. Lamb, *Eur. Phys. J.* **A52**, 63 (2016), [arXiv:1604.03894 \[astro-ph.HE\]](#).
 - [6] F. Özel and P. Freire, *Ann. Rev. Astron. Astrophys.* **54**, 401 (2016), [arXiv:1603.02698 \[astro-ph.HE\]](#).
 - [7] H. T. Cromartie *et al.*, *Nat. Astron.* **4**, 72 (2019), [arXiv:1904.06759 \[astro-ph.HE\]](#).
 - [8] B. P. Abbott *et al.* (LIGO Scientific Collaboration, Virgo Collaboration), *Phys. Rev. Lett.* **119**, 161101 (2017), [arXiv:1710.05832 \[gr-qc\]](#).
 - [9] B. P. Abbott *et al.* (LIGO Scientific Collaboration, Virgo Collaboration), *Phys. Rev.* **X9**, 011001 (2019), [arXiv:1805.11579 \[gr-qc\]](#).
 - [10] B. P. Abbott *et al.* (LIGO Scientific Collaboration, Virgo Collaboration), *Phys. Rev. Lett.* **121**, 161101 (2018), [arXiv:1805.11581 \[gr-qc\]](#).
 - [11] B. Abbott *et al.* (LIGO Scientific Collaboration, Virgo Collaboration), *Astrophys. J. Lett.* **892**, L3 (2020), [arXiv:2001.01761 \[astro-ph.HE\]](#).
 - [12] B. Margalit and B. D. Metzger, *Astrophys. J.* **850**, L19 (2017), [arXiv:1710.05938 \[astro-ph.HE\]](#).
 - [13] A. Bauswein, O. Just, H.-T. Janka, and N. Stergioulas, *Astrophys. J.* **850**, L34 (2017), [arXiv:1710.06843 \[astro-ph.HE\]](#).
 - [14] M. W. Coughlin, T. Dietrich, B. Margalit, and B. D. Metzger, *Mon. Not. Roy. Astron. Soc.* **489**, L91 (2019), [arXiv:1812.04803 \[astro-ph.HE\]](#).
 - [15] G. Raaijmakers *et al.*, (2019), [arXiv:1912.11031 \[astro-ph.HE\]](#).
 - [16] P. Landry, R. Essick, and K. Chatziioannou, (2020), [arXiv:2003.04880 \[astro-ph.HE\]](#).
 - [17] G. Pratten, P. Schmidt, and T. Hinderer, (2019), [arXiv:1905.00817 \[gr-qc\]](#).

- [18] S. Ma, H. Yu, and Y. Chen, (2020), [arXiv:2003.02373 \[gr-qc\]](#).
- [19] N. N. Weinberg, *Astrophys. J.* **819**, 109 (2016), [arXiv:1509.06975 \[astro-ph.SR\]](#).
- [20] B. P. Abbott *et al.* (LIGO Scientific Collaboration, Virgo Collaboration), *Phys. Rev. Lett.* **122**, 061104 (2019), [arXiv:1808.08676 \[astro-ph.HE\]](#).
- [21] É. É. Flanagan and T. Hinderer, *Phys. Rev. D* **77**, 021502 (2008), [arXiv:0709.1915 \[astro-ph\]](#).
- [22] Z.-G. Xing, J. M. Centrella, and S. L. W. McMillan, *Phys. Rev. D* **50**, 6247 (1994), [arXiv:gr-qc/9411029 \[gr-qc\]](#).
- [23] M. Shibata, K. Taniguchi, and K. Uryu, *Phys. Rev. D* **71**, 084021 (2005), [arXiv:gr-qc/0503119](#).
- [24] M. Shibata and K. Taniguchi, *Phys. Rev. D* **73**, 064027 (2006).
- [25] R. Oechslin and H.-T. Janka, *Phys. Rev. Lett.* **99**, 121102 (2007), [arXiv:astro-ph/0702228](#).
- [26] K. Hotokezaka, K. Kyutoku, H. Okawa, M. Shibata, and K. Kiuchi, *Phys. Rev. D* **83**, 124008 (2011), [arXiv:1105.4370 \[astro-ph.HE\]](#).
- [27] A. Bauswein and H.-T. Janka, *Physical Review Letters* **108**, 011101 (2012), [arXiv:1106.1616 \[astro-ph.SR\]](#).
- [28] A. Bauswein, H. Janka, K. Hebeler, and A. Schwenk, *Phys. Rev. D* **86**, 063001 (2012), [arXiv:1204.1888 \[astro-ph.SR\]](#).
- [29] K. Hotokezaka, K. Kiuchi, K. Kyutoku, H. Okawa, Y.-i. Sekiguchi, M. Shibata, and K. Taniguchi, *Phys. Rev. D* **87**, 024001 (2013), [arXiv:1212.0905 \[astro-ph.HE\]](#).
- [30] K. Takami, L. Rezzolla, and L. Baiotti, *Physical Review Letters* **113**, 091104 (2014), [arXiv:1403.5672 \[gr-qc\]](#).
- [31] S. Bernuzzi, T. Dietrich, and A. Nagar, *Physical Review Letters* **115**, 091101 (2015), [arXiv:1504.01764 \[gr-qc\]](#).
- [32] A. Bauswein and N. Stergioulas, *Phys. Rev. D* **91**, 124056 (2015).
- [33] F. Foucart, R. Haas, M. D. Duez, E. O'Connor, C. D. Ott, L. Roberts, L. E. Kidder, J. Lippuner, H. P. Pfeiffer, and M. A. Scheel, *Phys. Rev. D* **93**, 044019 (2016), [arXiv:1510.06398 \[astro-ph.HE\]](#).
- [34] L. Lehner, S. L. Liebling, C. Palenzuela, O. L. Caballero, E. O'Connor, M. Anderson, and D. Neilsen, *Class. Quant. Grav.* **33**, 184002 (2016), [arXiv:1603.00501 \[gr-qc\]](#).
- [35] W. E. East, V. Paschalidis, and F. Pretorius, *Classical and Quantum Gravity* **33**, 244004 (2016), [arXiv:1609.00725 \[astro-ph.HE\]](#).
- [36] T. Dietrich, M. Ujevic, W. Tichy, S. Bernuzzi, and B. Brügmann, *Phys. Rev. D* **95**, 024029 (2017), [arXiv:1607.06636 \[gr-qc\]](#).
- [37] N. Stergioulas, A. Bauswein, K. Zagkouris, and H.-T. Janka, *Mon. Not. Roy. Astron. Soc.* **418**, 427 (2011), [arXiv:1105.0368 \[gr-qc\]](#).
- [38] A. Bauswein, N. Stergioulas, and H.-T. Janka, *Eur. Phys. J. A* **52**, 56 (2016), [arXiv:1508.05493 \[astro-ph.HE\]](#).
- [39] S. De, D. Finstad, J. M. Lattimer, D. A. Brown, E. Berger, and C. M. Biwer, *Phys. Rev. Lett.* **121**, 091102 (2018), [Erratum: *Phys. Rev. Lett.* 121, no. 25, 259902 (2018)], [arXiv:1804.08583 \[astro-ph.HE\]](#).
- [40] L. Dai, T. Venumadhav, and B. Zackay, (2018), [arXiv:1806.08793 \[gr-qc\]](#).
- [41] B. P. Abbott *et al.* (LIGO Scientific Collaboration, Virgo Collaboration), *The Astrophysical Journal* **851**, L16 (2017).
- [42] B. P. Abbott *et al.* (LIGO Scientific Collaboration, Virgo Collaboration), *Living Rev. Rel.* **19**, 1 (2013), [arXiv:1304.0670 \[gr-qc\]](#).
- [43] R. Lynch, S. Vitale, L. Barsotti, S. Dwyer, and M. Evans, *Phys. Rev. D* **91**, 044032 (2015), [arXiv:1410.8503 \[gr-qc\]](#).
- [44] M. Tse *et al.*, *Phys. Rev. Lett.* **123**, 231107 (2019).
- [45] L. McCuller *et al.*, (2020), [arXiv:2003.13443 \[astro-ph.IM\]](#).
- [46] H. Yang, V. Paschalidis, K. Yagi, L. Lehner, F. Pretorius, and N. Yunes, *Phys. Rev. D* **97**, 024049 (2018), [arXiv:1707.00207 \[gr-qc\]](#).
- [47] S. Bose, K. Chakravarti, L. Rezzolla, B. S. Sathyaprakash, and K. Takami, *Phys. Rev. Lett.* **120**, 031102 (2018), [arXiv:1705.10850 \[gr-qc\]](#).
- [48] K. Chatzioannou, J. A. Clark, A. Bauswein, M. Millhouse, T. B. Littenberg, and N. Cornish, *Phys. Rev. D* **96**, 124035 (2017), [arXiv:1711.00040 \[gr-qc\]](#).
- [49] A. Torres-Rivas, K. Chatzioannou, A. Bauswein, and J. A. Clark, *Phys. Rev. D* **99**, 044014 (2019), [arXiv:1811.08931 \[gr-qc\]](#).
- [50] D. Martynov *et al.*, *Phys. Rev. D* **99**, 102004 (2019), [arXiv:1901.03885 \[astro-ph.IM\]](#).
- [51] B. P. Abbott *et al.* (LIGO Scientific Collaboration), *Class. Quant. Grav.* **34**, 044001 (2017), [arXiv:1607.08697 \[astro-ph.IM\]](#).
- [52] D. Reitze *et al.*, *Bull. Am. Astron. Soc.* **51**, 141 (2019), [arXiv:1903.04615 \[astro-ph.IM\]](#).
- [53] D. Reitze *et al.*, *Bull. Am. Astron. Soc.* **51**, 035 (2019), [arXiv:1907.04833 \[astro-ph.IM\]](#).
- [54] M. Punturo *et al.*, *Class. Quant. Grav.* **27**, 194002 (2010).
- [55] M. Maggiore *et al.*, (2019), [arXiv:1912.02622 \[astro-ph.CO\]](#).
- [56] S. Sachdev, T. Regimbau, and B. S. Sathyaprakash, *ArXiv e-Prints* (2020), [arXiv:2002.05365 \[gr-qc\]](#).
- [57] B. P. Abbott *et al.* (LIGO Scientific Collaboration, Virgo Collaboration), *Phys. Rev. Lett.* **120**, 091101 (2018), [arXiv:1710.05837 \[gr-qc\]](#).
- [58] B. P. Abbott *et al.* (LIGO Scientific Collaboration, Virgo Collaboration), *Phys. Rev. D* **99**, 031040 (2019), [arXiv:1811.12907 \[astro-ph.HE\]](#).
- [59] C. J. Moore, R. H. Cole, and C. P. L. Berry, *Class. Quant. Grav.* **32**, 015014 (2015), [arXiv:1408.0740 \[gr-qc\]](#).
- [60] B. D. Lackey, M. Nayyar, and B. J. Owen, *Phys. Rev. D* **73**, 024021 (2006), [arXiv:astro-ph/0507312 \[astro-ph\]](#).
- [61] P. Madau and M. Dickinson, *Ann. Rev. Astron. Astrophys.* **52**, 415 (2014), [arXiv:1403.0007 \[astro-ph.CO\]](#).
- [62] M. Favata, *Phys. Rev. Lett.* **112**, 101101 (2014), [arXiv:1310.8288 \[gr-qc\]](#).
- [63] L. Wade, J. D. Creighton, E. Ochsner, B. D. Lackey, B. F. Farr, *et al.*, *Phys. Rev. D* **89**, 103012 (2014), [arXiv:1402.5156 \[gr-qc\]](#).
- [64] M. Vallisneri, *Phys. Rev. D* **77**, 042001 (2008), [arXiv:gr-qc/0703086 \[GR-QC\]](#).
- [65] B. Bécsy and N. J. Cornish, (2019), [arXiv:1912.08807 \[gr-qc\]](#).
- [66] W. Del Pozzo, T. G. F. Li, M. Agathos, C. Van Den Broeck, and S. Vitale, *Phys. Rev. Lett.* **111**, 071101 (2013), [arXiv:1307.8338 \[gr-qc\]](#).
- [67] K. Yagi and N. Yunes, *Class. Quant. Grav.* **33**, 13LT01

- (2016), arXiv:1512.02639 [gr-qc].
- [68] K. Chatziioannou, C.-J. Haster, and A. Zimmerman, *Phys. Rev. D* **97**, 104036 (2018), arXiv:1804.03221 [gr-qc].
- [69] C. Raithel, F. Özel, and D. Psaltis, *Astrophys. J.* **857**, L23 (2018), arXiv:1803.07687 [astro-ph.HE].
- [70] B. Kumar and P. Landry, *Phys. Rev.* **D99**, 123026 (2019), arXiv:1902.04557 [gr-qc].
- [71] M. Oertel, M. Hempel, T. Klähn, and S. Typel, *Rev. Mod. Phys.* **89**, 015007 (2017), arXiv:1610.03361 [astro-ph.HE].
- [72] G. Montaña, L. Tolós, M. Hanauske, and L. Rezzolla, *Phys. Rev. D* **99**, 103009 (2019), arXiv:1811.10929 [astro-ph.HE].
- [73] R. Essick, P. Landry, and D. E. Holz, *Phys. Rev. D* **101**, 063007 (2020), arXiv:1910.09740 [astro-ph.HE].
- [74] H.-Y. Chen, P. M. Chesler, and A. Loeb, *Astrophys. J.* **893**, L4 (2020), arXiv:1909.04096 [astro-ph.HE].
- [75] K. Chatziioannou and S. Han, *Phys. Rev.* **D101**, 044019 (2020), arXiv:1911.07091 [gr-qc].
- [76] J. S. Read, B. D. Lackey, B. J. Owen, and J. L. Friedman, *Phys. Rev. D* **79**, 124032 (2009), arXiv:0812.2163 [astro-ph].
- [77] B. D. Lackey and L. Wade, *Phys. Rev. D* **91**, 043002 (2015), arXiv:1410.8866 [gr-qc].
- [78] L. Lindblom, *Phys. Rev.* **D97**, 123019 (2018), arXiv:1804.04072 [astro-ph.HE].
- [79] M. F. Carney, L. E. Wade, and B. S. Irwin, *Phys. Rev.* **D98**, 063004 (2018), arXiv:1805.11217 [gr-qc].
- [80] C. A. Raithel, F. Özel, and D. Psaltis, *Astrophys. J.* **831**, 44 (2016), arXiv:1605.03591 [astro-ph.HE].
- [81] I. Tews, J. Carlson, S. Gandolfi, and S. Reddy, *Astrophys. J.* **860**, 149 (2018), arXiv:1801.01923 [nucl-th].
- [82] S. K. Greif, G. Raaijmakers, K. Hebeler, A. Schwenk, and A. L. Watts, *Mon. Not. Roy. Astron. Soc.* **485**, 5363 (2019), arXiv:1812.08188 [astro-ph.HE].
- [83] M. G. Alford and S. Han, *Eur. Phys. J.* **A52**, 62 (2016), arXiv:1508.01261 [nucl-th].
- [84] S. Han and A. W. Steiner, *Phys. Rev. D* **99**, 083014 (2019), arXiv:1810.10967 [nucl-th].
- [85] R. B. Wiringa, V. Fiks, and A. Fabrocini, *Phys. Rev. C* **38**, 1010 (1988).
- [86] F. Gulminelli and A. R. Raduta, *Phys. Rev. C* **92**, 055803 (2015), arXiv:1504.04493 [nucl-th].
- [87] P. Danielewicz and J. Lee, *Nucl. Phys. A* **818**, 36 (2009), arXiv:0807.3743 [nucl-th].
- [88] B. P. Abbott *et al.* (LIGO Scientific Collaboration, Virgo Collaboration), *Class. Quant. Grav.* **37**, 045006 (2020), arXiv:1908.01012 [gr-qc].
- [89] J. Alsing, H. O. Silva, and E. Berti, *Mon. Not. Roy. Astron. Soc.* **478**, 1377 (2018), arXiv:1709.07889 [astro-ph.HE].
- [90] M. Dominik, K. Belczynski, C. Fryer, D. Holz, E. Berti, T. Bulik, I. Mandel, and R. O’Shaughnessy, *Astrophys. J.* **759**, 52 (2012), arXiv:1202.4901 [astro-ph.HE].
- [91] T. Dietrich *et al.*, *Phys. Rev.* **D99**, 024029 (2019), arXiv:1804.02235 [gr-qc].
- [92] Cosmic Explorer Project, “Cosmic explorer,” (2019).
- [93] S. Droz, D. J. Knapp, E. Poisson, and B. J. Owen, *Phys. Rev.* **D59**, 124016 (1999), arXiv:gr-qc/9901076 [gr-qc].
- [94] K. Takami, L. Rezzolla, and L. Baiotti, *Phys. Rev. Lett.* **113**, 091104 (2014), arXiv:1403.5672 [gr-qc].
- [95] J. A. Clark, A. Bauswein, N. Stergioulas, and D. Shoemaker, *Class. Quant. Grav.* **33**, 085003 (2016), arXiv:1509.08522 [astro-ph.HE].
- [96] J. Wilson, G. Mathews, and P. Marronetti, *Phys. Rev. D* **54**, 1317 (1996), arXiv:gr-qc/9601017.
- [97] R. Oechslin, S. Rosswog, and F. K. Thielemann, *Phys. Rev. D* **65**, 103005 (2002), arXiv:gr-qc/0111005.
- [98] R. Oechslin, H.-T. Janka, and A. Marek, *Astron. Astrophys.* **467**, 395 (2007), arXiv:astro-ph/0611047.
- [99] A. Bauswein, H.-T. Janka, and R. Oechslin, *Phys. Rev. D* **82**, 084043 (2010), arXiv:1006.3315 [astro-ph.SR].
- [100] K. W. Tsang, T. Dietrich, and C. Van Den Broeck, *Phys. Rev.* **D100**, 044047 (2019), arXiv:1907.02424 [gr-qc].
- [101] M. Breschi, S. Bernuzzi, F. Zappa, M. Agathos, A. Perego, D. Radice, and A. Nagar, *Phys. Rev.* **D100**, 104029 (2019), arXiv:1908.11418 [gr-qc].
- [102] S. Bernuzzi *et al.*, (2020), arXiv:2003.06015 [astro-ph.HE].
- [103] A. Bauswein, T. W. Baumgarte, and H. T. Janka, *Phys. Rev. Lett.* **111**, 131101 (2013), arXiv:1307.5191 [astro-ph.SR].
- [104] A. Bauswein, S. Blacker, V. Vijayan, N. Stergioulas, K. Chatziioannou, J. A. Clark, N.-U. F. Bastian, D. B. Blaschke, M. Cierniak, and T. Fischer, (2020), arXiv:2004.00846 [astro-ph.HE].
- [105] E. D. Hall, (2020), private communication.
- [106] Both Cosmic Explorer configurations explored here assume a 1.4% transmissivity of the input test mass, and a 2% transmissivity of the signal-recycling mirror.
- [107] M. Evans, R. Sturani, S. Vitale, and E. Hall, *Unofficial sensitivity curves (ASD) for aLIGO, Kagra, Virgo, Voyager, Cosmic Explorer and ET*, Tech. Rep. (2018).
- [108] R. X. Adhikari *et al.* (LIGO), (2020), arXiv:2001.11173 [astro-ph.IM].
- [109] J. Aasi *et al.* (LIGO Scientific Collaboration), *Class. Quant. Grav.* **32**, 074001 (2015), arXiv:1411.4547 [gr-qc].
- [110] L. Barsotti, P. Fritschel, M. Evans, and S. Gras, *Updated Advanced LIGO sensitivity design curve*, Tech. Rep. (2018).
- [111] M. Bailes *et al.*, (2019), arXiv:1912.06305 [astro-ph.IM].
- [112] D. D. Brown, (2020), private communication, OzGrav, LIGO DCC-T2000062.
- [113] K. Cannon *et al.*, *Astrophys. J.* **748**, 136 (2012), arXiv:1107.2665 [astro-ph.IM].
- [114] D. Meacher, K. Cannon, C. Hanna, T. Regimbau, and B. Sathyaprakash, *Phys. Rev. D* **93**, 024018 (2016), arXiv:1511.01592 [gr-qc].
- [115] F. Hernandez Vivanco, R. Smith, E. Thrane, and P. D. Lasky, *Phys. Rev.* **D100**, 043023 (2019), arXiv:1903.05778 [gr-qc].
- [116] A. Bauswein, N.-U. F. Bastian, D. B. Blaschke, K. Chatziioannou, J. A. Clark, T. Fischer, and M. Oertel, *Phys. Rev. Lett.* **122**, 061102 (2019), arXiv:1809.01116 [astro-ph.HE].
- [117] C. Messenger and J. Read, *Phys. Rev. Lett.* **108**, 091101 (2012), arXiv:1107.5725 [gr-qc].
- [118] C. Messenger, K. Takami, S. Gossan, L. Rezzolla, and B. S. Sathyaprakash, *Phys. Rev.* **X4**, 041004 (2014), arXiv:1312.1862 [gr-qc].
- [119] W. Del Pozzo, T. G. F. Li, and C. Messenger, *Phys. Rev.* **D95**, 043502 (2017), arXiv:1506.06590 [gr-qc].
- [120] R. Dudi, F. Pannarale, T. Dietrich, M. Hannam, S. Bernuzzi, F. Ohme, and B. Brügmann, *Phys. Rev.*

- D98**, 084061 (2018), [arXiv:1808.09749 \[gr-qc\]](#).
- [121] A. Samajdar and T. Dietrich, *Phys. Rev.* **D98**, 124030 (2018), [arXiv:1810.03936 \[gr-qc\]](#).
- [122] M. Pürrer and C.-J. Haster, (2019), [arXiv:1912.10055 \[gr-qc\]](#).
- [123] LIGO Scientific Collaboration, “LIGO Algorithm Library - LALSuite,” free software (GPL) (2018).
- [124] T. P. Robitaille *et al.* (Astropy), *Astron. Astrophys.* **558**, A33 (2013), [arXiv:1307.6212 \[astro-ph.IM\]](#).
- [125] A. Price-Whelan *et al.*, *Astron. J.* **156**, 123 (2018), [arXiv:1801.02634](#).
- [126] T. Oliphant, “NumPy: A guide to NumPy,” USA: Trelgol Publishing (2006–), [Online; accessed *jtodayi*].
- [127] P. Virtanen *et al.*, *Nature Meth.* **17**, 261 (2020), [arXiv:1907.10121 \[cs.MS\]](#).
- [128] J. D. Hunter, *Comput. Sci. Eng.* **9**, 90 (2007).